Drought Variability over the Conterminous United States for the Past Century

LU SU,[a] QIAN CAO,[a] MU XIAO,[a,f] DAVID M. MOCKO,[b] MICHAEL BARLAGE,[c,g] DONGYUE LI,[a] CHRISTA D. PETERS-LIDARD,[d] AND DENNIS P. LETTENMAIER[a]

[a] *Department of Geography, University of California, Los Angeles, Los Angeles, California*
[b] *Science Applications International Corporation, Hydrological Sciences Laboratory, NASA Goddard Space Flight Center, Greenbelt, Maryland*
[c] *Research Applications Laboratory, National Center for Atmospheric Research, Boulder, Colorado*
[d] *Earth Sciences Division, NASA Goddard Space Flight Center, Greenbelt, Maryland*

(Manuscript received 30 June 2020, in final form 11 February 2021)

ABSTRACT: We examine the drought variability over the conterminous United States (CONUS) for 1915–2018 using the Noah-MP land surface model. We examine different model options on drought reconstruction, including optional representation of groundwater and dynamic vegetation phenology. Over our 104-yr reconstruction period, we identify 12 great droughts that each covered at least 36% of CONUS and lasted for at least 5 months. The great droughts tend to have smaller areas when groundwater and/or dynamic vegetation are included in the model configuration. We detect a small decreasing trend in dry area coverage over CONUS in all configurations. We identify 45 major droughts in the baseline (with a dry area coverage greater than 23.6% of CONUS) that are, on average, somewhat less severe than great droughts. We find that representation of groundwater tends to increase drought duration for both great and major droughts, primarily by leading to earlier drought onset (some due to short-lived recovery from a previous drought) or later demise (groundwater anomalies lag precipitation anomalies). In contrast, representation of dynamic vegetation tends to shorten major droughts duration, primarily due to earlier drought demise (closed stoma or dead vegetation reduces ET loss during droughts). On a regional basis, the U.S. Southwest (Southeast) has the longest (shortest) major drought durations. Consistent with earlier work, dry area coverage in all subregions except the Southwest has decreased. The effects of groundwater and dynamic vegetation vary regionally due to differences in groundwater depths (hence connectivity with the surface) and vegetation types.

KEYWORDS: Drought; Hydrology; Soil moisture; Land surface model

1. Introduction

Drought is among the most costly natural disasters (Wilhite 2006; Wu et al. 2018). It is estimated that the 27 drought events between 1980 and 2020 cost the United States at least $252 billion (in 2020 dollars) with an average cost of more than $9.3 billion incurred during each event (NOAA 2020). Drought losses from the 1988 drought in the conterminous United States (CONUS) alone cost nearly $44.4 billion (NOAA 2020). The more recent 2012 drought, which covered more than 62% of CONUS, had losses of $33.9 billion (NOAA 2020). Agriculture is usually the economic sector most severely impacted by droughts due to its dependence on water resources and soil moisture reserves during various stages of crop growth (Narasimhan and Srinivasan 2005). The large losses associated with drought inspire research to better understand the mechanisms that underlie drought events, which should help in planning to mitigate drought impacts.

Motivated by the recent history of drought in the United States, we examine the characteristics of CONUS droughts over the past century. Drought areal coverage is an important drought attribute; widespread droughts tend to have greater impacts. Furthermore, Mo and Lettenmaier (2018) found, in an analysis of 16 CONUS droughts with large areal coverage, that most of the abovementioned droughts with large spatial coverage affected substantial parts of the central United States with the country's greatest agricultural production.

Results of recent research differ as to whether droughts have become more frequent or severe in recent decades (Dai et al. 2004; Andreadis and Lettenmaier 2006; Mo and Lettenmaier 2018). An interesting question that we address here is whether there are trends in the drought area coverage over the past century. Climate and land surface conditions vary greatly in different regions of CONUS, and hence drought characteristics vary as well (Ge et al. 2016; Ahmadalipour et al. 2017). Drought

Supplemental information related to this paper is available at the Journals Online website: https://doi.org/10.1175/JHM-D-20-0158.s1.

[f] Current affiliation: School of Sustainable Engineering and the Built Environment, Arizona State University, Tempe, Arizona.
[g] Current affiliation: Environmental Modeling Center, NOAA/National Centers for Environmental Prediction, College Park, Maryland.

Corresponding author: Dennis P. Lettenmaier, dlettenm@ucla.edu

DOI: 10.1175/JHM-D-20-0158.1

duration is another key attribute that determines the impact of drought, which leads to the related question addressed in this work: How have drought durations varied over the last century?

The U.S. Drought Monitor (USDM; Svoboda et al. 2002) is widely used to assess the coverage and intensity of drought across the CONUS. However, the weekly USDM maps are not based on an algorithm, but rather on professional opinion, and are therefore subjective and not reproducible. This has motivated various alternative objective drought monitors, such as the North American Land Data Assimilation System (NLDAS; Mitchell et al. 2004; Xia et al. 2012a,b) drought monitor hosted by NASA (https://ldas.gsfc.nasa.gov/nldas/drought-monitor), and UCLA's Experimental Surface Water Monitor (www.hydro.ucla.edu/SurfaceWaterGroup/monitors.php) (Wang et al. 2009), both of which are based on model-predicted quantities such as soil moisture (SM) and snow water equivalent (SWE). We note that the USDM began in 1999, and does not include the long reconstruction period covered by this study. The NLDAS drought monitor likewise spans a considerably shorter record than the century-plus period that we examine here.

SM is an important drought indicator, especially for agricultural droughts. Two critical elements that affect SM dynamics are the distribution of shallow groundwater and vegetation (Fan et al. 2013; Fan 2015; Verstraeten et al. 2008; Dickinson et al. 1998). Shallow unconfined aquifers affect SM close to the land surface, as groundwater can reduce or even reverse the downward flux (drainage) of moisture from the surface (Barlage et al. 2015; Martinez et al. 2016). In addition, where groundwater is shallow, or where roots are deep enough, groundwater can be accessed directly by plants, affecting the fluxes of moisture via transpiration (Fan 2015). However, the abovementioned objective drought monitors do not currently consider groundwater, nor have many studies of drought trends (e.g., Mo and Lettenmaier 2018; Mo et al. 2011; Mo 2008; Xiao et al. 2016). On the other hand, groundwater conditions are known to affect drought onset, persistence, and demise (Bloomfield and Marchant 2013; Hughes et al. 2012; Peters et al. 2003, 2005).

Vegetation influences SM via evapotranspiration (ET). Simulation of SM depends on knowledge of vegetation features, including stomatal conductance and leaf area index (LAI), which affect transpiration and interception evaporation, and vegetation height, which is reflected in aerodynamic resistance, which in turn affects both canopy evaporation and transpiration. Nonetheless, the land surface models used in the abovementioned objective drought monitors all use prescribed vegetation characteristics (e.g., fixed seasonal cycles of fractional vegetation coverage and/or LAI). These models have the same vegetation values every year, which can continue to generate anomalously high ET during dry conditions and erroneously exacerbate soil moisture deficits. Vegetation is immediately available for ET after cessation of a drought or a long dry season (Dickinson et al. 1998), which is a dubious simplification of reality in many cases.

Using land surface models that are representative of the physical processes that affect drought should be beneficial to drought representation. The new U.S. National Water Model (NWM; Cosgrove and Gochis 2018) (http://water.noaa.gov/about/nwm) uses the Noah Multiparameterization (Noah-MP) land surface model (LSM) (Niu et al. 2011) as the soil (and optionally groundwater) vertical column LSM component. Although the current "standard" NWM configuration does not use these options, Noah-MP has the ability to simulate groundwater and dynamic vegetation phenology as they affect land surface fluxes and storage of water, including SM (Niu et al. 2011). We would like to understand how these processes, not represented in previous drought reconstructions, affect drought identification, and in turn the motivating questions discussed above.

Given this background, our objectives here are to use Noah-MP to examine: 1) drought area coverage over CONUS and six subregions thereof over the period 1915–2018; 2) variations in drought duration over the CONUS and subregions; 3) identification of great droughts of the last century over CONUS; and 4) the impacts of representations of dynamic vegetation phenology and groundwater on drought area coverage, duration, and identification. In the remainder of this paper, we discuss development of Noah-MP model forcings in section 2. In section 3, we discuss our experimental design, and the role of the Noah-MP model. In section 4, we interpret and discuss our results, and we summarize and conclude in section 5.

2. Forcing description

The model's surface meteorological forcings are hourly precipitation P, near-surface temperature, near-surface wind, near-surface humidity, downward shortwave and longwave radiation, and surface pressure. Our preparation of forcings across the CONUS mainly consisted of two steps: 1) prepare the daily maximum and minimum near-surface temperature (Tmax and Tmin), P, and wind; 2) disaggregate the daily data into required hourly forcings. We took daily Tmax, Tmin, P, and wind from a consistent, long-term (1915–2011), fine-resolution (1/16° latitude–longitude) dataset for the entire CONUS from Livneh et al. (2013, hereafter L13). The L13 forcing data span the major droughts of the 1930s and 1950s, but miss the more recent 2012 CONUS drought and the 2012–16 California drought. Because we aim to conduct a comprehensive study of droughts over the past century, we used the available data from L13 (1915–2011) and extended the L13 forcings through 2018. In the forcing extension, we followed the same methods and used the same scripts as were used in L13. We gridded Tmax, Tmin, and P at a spatial resolution of 1/16° latitude–longitude with station data taken from approximately 20 000 NOAA Cooperative Observer (COOP) stations (mostly the same as in L13). Wind data were linearly interpolated from the (approximately 1.98° latitude–longitude) NCEP–NCAR reanalysis data (Kalnay et al. 1996). As in the original L13 dataset, we only used stations with at least 20 years of valid data. For consistency, we scaled the gridded precipitation values based on a 1961–90 Parameter-Elevation Regressions on Independent Slopes Model (PRISM; Daly et al. 1994) monthly climatology. Readers are referred to L13 for more details about the gridding methodology.

We conducted a forcing evaluation which showed that the extended forcing data are consistent with the original dataset (see Figs. S1 and S2 in the online supplemental material) in an overlap period (1961–2011). After the forcing data were extended, we aggregated the forcings to 1/8° latitude/longitude both to reduce computational demands and to be on same grid

TABLE 1. Noah-MP parameterization options used in this study.

Physical process representations	BASE	DYVEG2	DYVEG5	GW	DVGW
Dynamic vegetation phenology	Table LAI, FVEG[a] = max vegetation fraction (SHDMAX[b])	Dynamically predicted LAI, FVEG = $1 - e^{-0.52(\mathrm{LAI}+\mathrm{SAI})}$	Dynamically predicted LAI, FVEG = SHDMAX	Table LAI, FVEG = SHDMAX	Dynamically predicted LAI, FVEG = $1 - e^{-0.52(\mathrm{LAI}+\mathrm{SAI})}$
Runoff and groundwater	Free drainage at soil lower boundary			SIMGM	

[a] We show the comparison for the FVEG maps (averaged over 1915–2018) in BASE, DYVEG2, and DYVEG5 for two example months in Fig. S4.
[b] The SHDMAX map is shown in Fig. S3.

as the NLDAS forcing data (https://ldas.gsfc.nasa.gov/nldas/v2/forcing) and the NLDS drought monitor (Ek et al. 2011). We then applied the MTCLIM algorithms (Kimball et al. 1997; Thornton and Running 1999) for computation of specific humidity and downward solar radiation, respectively, and the Tennessee Valley Authority algorithm (Bras 1990) to compute downward longwave radiation (see Bohn et al. 2013 for details). We estimated surface air pressure based on grid cell elevation and global mean pressure lapse rates. Finally, we converted the daily data to hourly using a cubic spline to interpolate between Tmax and Tmin, and from which the other variables were derived using methods described by Bohn et al. (2013). We apportioned the daily precipitation into hourly intervals based on gridded hourly to daily observed precipitation ratios (the precipitation ratio calculation process is described in detail in Text 1 in the supplemental material).

3. Model configuration and experimental design

Noah-MP is a new-generation LSM, which is coupled to the Weather Research and Forecasting (WRF) regional atmospheric model in the NWM. Noah-MP extends the capabilities of the Noah LSM (Chen et al. 1996; Chen and Dudhia 2001) and incorporates multiple options for key land–atmosphere interaction processes, such as surface water infiltration, runoff, groundwater transfer, and options for representing snow albedo and vegetation growth (Niu et al. 2007; Niu et al. 2011). Here we used only Noah-MP, with its forcings provided by observations as described above, rather than in the coupled mode with WRF.

Noah-MP can be executed by prescribing both the horizontal and vertical density of vegetation using either ground- or satellite-based observations. Another available option is for prognostic vegetation growth that combines a Ball–Berry photosynthesis-based stomatal resistance (Ball et al. 1987) with a dynamic vegetation phenology model (Dickinson et al. 1998) that allocates carbon to various parts of vegetation (leaf, stem, wood, and root) and soil carbon pools (fast and slow), which allows a dynamic simulation of LAI. This CO_2-assimilation-based photosynthesis model is capable of distinguishing between C_3 and C_4 photosynthesis pathways and defines vegetation-specific parameters for plant photosynthesis and respiration. Carbon assimilation is controlled by several environmental conditions, including temperature, soil moisture availability and antecedent LAI, which affects radiation absorption. Leaf carbon stores are a balance between photosynthetic assimilation and losses due to respiration, turnover, and die-off. Die-off is the sum of processes related to soil moisture deficit and high/low temperature, both important during drought events. The model can also simulate unconfined groundwater using a simple groundwater model (SIMGM) (Niu et al. 2007), which represents recharge and discharge processes in an unconfined aquifer, added as a single integration element below the model's bottom soil layer. The temporal variation of water stored in the aquifer is determined by the residual of calculated recharge rate from the soil above minus the calculated discharge rate from the aquifer out of the grid. All model configurations have vegetation-dependent root depths, typically 2 m for trees and 1 m for short vegetation.

To understand the effects of dynamic vegetation phenology and groundwater on drought classification, we designed five experiments using Noah-MP version 4.0.1: 1) a baseline run (BASE) with prescribed LAI and a free drainage soil column lower boundary (does not include groundwater or dynamic vegetation phenology); 2) a groundwater (GW) run using Noah-MP's implementation of the simple groundwater model (SIMGM) (Niu et al. 2007); 3) and 4) two dynamic vegetation phenology runs (DYVEG2 and DYVEG5) (note that these simulations do not include GW), both of which use Noah-MP's short-term dynamic vegetation phenology model, but with different alternatives for calculating green vegetation fraction (FVEG) (details of the differences between DYVEG2 and DYVEG5 are shown in Table 1); and 5) a combination of DYVEG2 and GW (DVGW). The LAI in the nondynamic phenology experiments is based on multiyear MODIS LAI climatology. In particular, monthly LAI varies among months (e.g., January and February) but is fixed for the same month in different years (e.g., January 1920 and January 2000). We tested the combination of DYVEG2 and GW and the combination of DYVEG5 and GW and found that the former combination results in larger differences (in, for instance, SM and ET) than considering dynamic vegetation phenology or groundwater alone, so we chose the former combination. The detailed Noah-MP physics options used in our study are listed in Table 1.

We formed the initial conditions for our Noah-MP simulations by conducting a model spinup. For the BASE simulation, we ran the model for 1915 iteratively 25 times (25 repetitions of the same year). For the other four runs, we first ran the model

from 1915 to 1970, and then iterated 30 times with 1915 (our rationale for the longer spinup was that the groundwater option requires longer to equilibrate; the dynamic vegetation phenology needs a shorter spinup time but we did the same as for GW for consistency). The spinup was iterated until the variables (e.g., water table depth, SWE, SM) reached equilibrium based on the criteria suggested by Cai et al. (2014). After spinup, we took the final values of storage variables such as SM, SWE, groundwater levels, and (in the case of dynamic vegetation runs) vegetation masses and the LAI and SAI (stem area index), as the initial values from runs for 1915–2018.

4. Results and discussion

a. Evaluation of model outputs

To test the robustness of Noah-MP, we compared streamflow, SWE, and SM outputs with observations under drought conditions. The observed streamflow data are from USGS gauges, mostly the MOPEX (Schaake et al. 2006) dataset (https://waterdata.usgs.gov/nwis). The observed SWE data are from the USDA/NRCS Snowpack Telemetry (SNOTEL) network (https://www.wcc.nrcs.usda.gov/snow/) and California Data Exchange Center (http://cdec.water.ca.gov/index.html). Soil moisture data are from USDA/NRCS SCAN (Soil Climate Analysis Network) sites (https://www.drought.gov/drought/data-gallery/soil-climate-analysis-network-scan). The observations, especially for soil moisture, are sparsely distributed and in most cases are only available for a decade or so at most. For SWE and streamflow, we limited our comparisons to stations with at least 30 years of data; for SM, we only used stations with at least 10 years of data. We compared the percentiles of observations and model output for selected droughts (see Figs. S5–S7). Our comparisons show that while there are anomalies (perhaps in observations as well as model output), in general the spatial patterns of abnormally low soil moisture and SWE in the Noah-MP model constructions are similar to those in the observations (see Figs. S5–S7). Thus, we concluded that the model outputs are sufficiently robust to support the analyses we report below.

b. Temporal variations of dry area coverage

As discussed above, SM is an important drought indicator, especially for agricultural droughts. Here, we define dry areas as areas (grid cells) where soil moisture is less than the 20th percentile compared to the entire simulation period. The 20th percentile is equivalent to D1 drought as used by the U.S. Drought Monitor (https://droughtmonitor.unl.edu/About/WhatistheUSDM.aspx). We archived the total column soil moisture percentiles (relative to that grid cell's and that day's total column SM history). (Note that we used a 5-day sliding window for the 1916–2017 reconstruction; thus we lose part of a year at the beginning and end of our 1915–2018 simulation period). For runs with different physical settings (DYVEG and GW), we calculated the percentiles based on each run's separate history. We tested an alternative strategy where the percentiles were all computed using the BASE history, but this resulted in peculiar percentiles in some cases since the SM had persistent differences among the runs, and we therefore opted to use percentiles calculated relative to each run's own history.

Once all the runs were archived, we computed dry areas (all grid cells with total column SM below the threshold) and computed the fraction of the CONUS area at each (monthly averaged) time step. The time series of the fraction of the CONUS with SM below the D1 threshold are shown in Fig. 1. The BASE results show that the largest areal coverage is about 60% and the median coverage is about 18%. We see large decadal as well as annual fluctuations especially around 1917–18, 1931–35, 1939–40, 1950–56, 1963, 1977–78, and 2012 when the areal coverages were high.

In the dynamic vegetation phenology simulations (Figs. 1a,b), the results are somewhat different. At first glance, the results shown in Fig. 1 (BASE compared with DYVEG2 and DYVEG5) appear quite similar. However, the difference time series (plotted as blue in Figs. 1a,b) show that the differences (especially for DYVEG2) can be as large as five percent of the area of CONUS. The dry area coverage in DYVEG2 is higher than BASE in some years, especially when the major droughts are more severe (in terms of area coverage, e.g., 1930s, 1950s, 1960s, 2000s) while lower in the rest of the years when drought areal coverage fraction is lower (e.g., 1940s, 1980s, 1990s). However, in another dynamic vegetation phenology run (DYVEG5), the differences are much smaller (Fig. 1b). DYVEG2 and DYVEG5 use different methods to calculate the green vegetation fraction (FVEG) as shown in Table 1 which results in different LAI and latent heat simulations especially for cropland. We found that the LAI in DYVEG5 is a little higher than in DYVEG2 in spring and summer and is generally similar for most vegetation types (Fig. S8) (the land cover types are mapped in Fig. S9). The differences are larger for cropland, where the LAI in cropland in DYVEG5 is much higher (and similar to BASE), while the LAI in DYVEG2 in cropland is significantly lower. The greater similarity in the LAI simulation in BASE and DYVEG5 results in smaller differences in the drought simulations in these two runs. To explore the effects of transient year-to-year variations in LAI in our analysis, we examined the linear Pearson correlation between the monthly LAI and SM anomaly (monthly LAI–LAI climatology) for 1915–2018 in BASE, DYVAEG2, and DYVEG5. We found that the correlations in BASE are not significantly different from 0 for almost all grid cells over CONUS (p value < 0.1), which is not surprising since the LAI in BASE is the prescribed monthly climatology. The linear correlations in both DYVEG2 and DYVEG5 are relatively small over large parts of CONUS (p value < 0.1) (Fig. S11). The correlations are higher in the southern CONUS with R ranging from 0.3 to 0.8 where shrubland is the dominate vegetation. A possible explanation is that shrubland LAI varies interannually and higher LAI helps to decrease ET from soil and thus has a strong positive effect on SM. The results show that the dynamically simulated LAI in DYVEG2/DYVEG5 is more highly correlated with SM than the prescribed LAI in BASE, with a much stronger relationship in the southern CONUS than in the remainder of the domain. The resulting

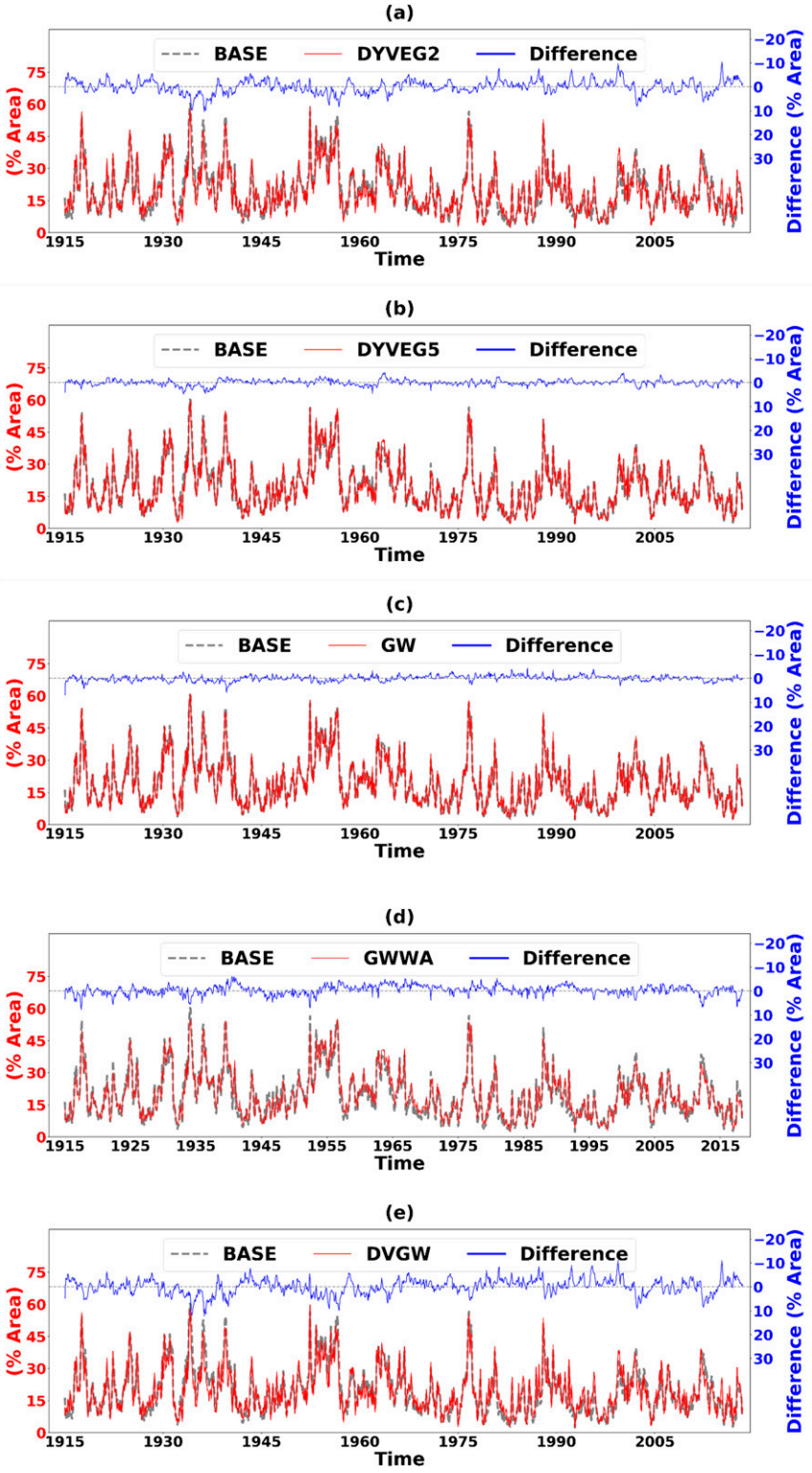

FIG. 1. (a) Dry area coverage, with BASE, DYVEG2, and differences. (b)–(e) As in (a), but that the red line is for DYVEG5, GW, GWWA, and DVGW, respectively. (Here GW is for SM analysis in GW, and GWWA is for SM + WA analysis in GW.)

TABLE 2. Duration, spatial extent, and severity of the great drought events. These are a union of 12 events classified based on BASE, DYVEG2, DYVEG5, DVGW SM, or GWWA outputs. Events classified in DYVEG/GWWA but not in BASE have an asterisk; all others are based on BASE. All values given are from the BASE run.

Events	Peak coverage date	Duration(months)	Spatial extent (% of CONUS)			Severity[a]		
			Mean	Max	Min	Mean	Max	Min
Dec 1917–Apr 1918	Jan 1918	5	46	55	42	15.4	7.1	17.8
Apr–Sep 1925*	Jun 1925	6	41	48	35	16.2	8.3	21.3
May–Nov 1931	Jul 1931	7	41	47	37	17.1	8.9	23.3
May–Nov 1934	Aug 1934	7	52	60	42	14.4	6.8	22.0
Jun–Dec 1936	Jul 1936	7	45	51	36	17.1	8.0	28.8
Oct 1939–Apr 1940	Jan 1940	7	45	53	36	17.3	8.6	24.9
Oct 1953–Apr 1954	Nov 1953	7	42	50	36	18.1	7.9	27.0
Jul 1954–May 1955	Aug 1954	11	41	45	36	18.1	8.6	26.3
Sep 1956–Mar 1957	Dec 1956	7	48	53	40	16.0	7.4	25.7
Nov 1963–Apr 1964*	Nov 1963	6	36	43	33	21.7	8.2	31.3
Dec 1976–Aug 1977	Feb 1977	9	47	54	38	17.2	6.2	26.8
Jul 2012–Dec 2012	Jul 2012	6	38	42	34	20.1	9.1	27.0

[a] Severity is expressed as the spatially averaged SM percentile relative to the study period. Greater percentiles mean lower severity.

differences in LAI presumably affect drought variability in the different model implementations. Tang et al. (2012) also found that VIC-simulated SM varied by using climatological LAI and interannually varying LAI in western Mexico for 2001–08 with a small regression slope.

The dry area based on SM percentiles for the groundwater run (GW) is very similar to BASE (Fig. 1c). However, the differences are somewhat larger if we calculate the dry area based on percentiles of the sum of groundwater and SM [water in aquifer (WA) + SM] for both GW and BASE (in BASE WA is constant in all grids and at all times, so the percentiles for only SM or WA + SM are the same in BASE; we denote the WA + SM in GW as GWWA to distinguish it from the analysis of only SM in GW) (Fig. 1d). Comparison of Fig. 1c (only considers SM) and Fig. 1d (considers SM + WA) shows that dynamic groundwater does not affect soil moisture percentiles much (notwithstanding that SIMGM represents some interactions between groundwater and the vadose zone), but significantly affects droughts by influencing groundwater storage (which can be considerably larger than SM). If we consider dynamic vegetation and groundwater simultaneously (DVGW) and compute dry area based on soil moisture (Fig. 1e), dry areas are quite similar to DYVEG2 (Fig. 1a).

Since groundwater closer to the surface is more relevant to agricultural drought than is deep groundwater, we inspected the difference in dry area in locations with deep/shallow groundwater levels. We divided the CONUS into two parts with water table depth (ZWT) greater/smaller than the median (2.73 m) of mean ZWT (over the study period) of all grids over CONUS. As expected, the differences of dry area between BASE and GW (Figs. S10a,b) are greater (with greater standard deviation) in places with shallow groundwater than with deep groundwater. However, if we calculate dry area based on GWWA (Figs. S10c,d), the magnitudes of differences are greater in areas with deep groundwater levels (with greater standard deviation); but the fluctuation frequency is higher where groundwater levels are shallow.

c. *Identification of great droughts*

In the interest of focusing on long-term severe droughts, we defined drought events as having SM percentiles below a threshold (20th percentile) and having durations longer than five months. We selected drought events for which the area under drought (across the entire CONUS domain) exceeded the 90th percentile (33% of CONUS, or 2.53×10^6 km^2) for the study period, which we define as great droughts. There were 10 qualifying events in BASE, which are listed in Table 2 (without superscripts). For each event, we listed the areal fraction of CONUS where SM percentiles < 20 and the spatial averaged monthly SM percentile for each month over the duration of drought. We then calculated the mean, maximum, and minimum coverages, and spatially averaged SM percentiles over the duration of that event within the maximum spatial extent. We applied the same identification approach to SM outputs for DYVEG2, DYVEG5, DVGW runs, and GWWA output for GW run and identified the great droughts for each run and output. For GWWA, we calculated the percentiles of the sum of moisture in the soil column and groundwater.

Most of the great droughts identified in these four runs also appeared in BASE, with two exceptions (April 1925–September 1925 and November 1963–April 1964) which are asterisked in Table 2. In total, we identified 12 great droughts. The SM percentiles for BASE averaged over the duration of each of the great drought events are given in Fig. 2. It should be noted that the mean provides only an approximation of drought location and coverage, because droughts often shift from one location to another, and the areal coverage can also change over the duration of an event. The spatial coverage was different for different drought events, but most of them covered the central CONUS (Fig. 2). This is in part by construct (large spatial coverage favors droughts centered on the central part of the domain); however, Mo and Lettenmaier (2018)

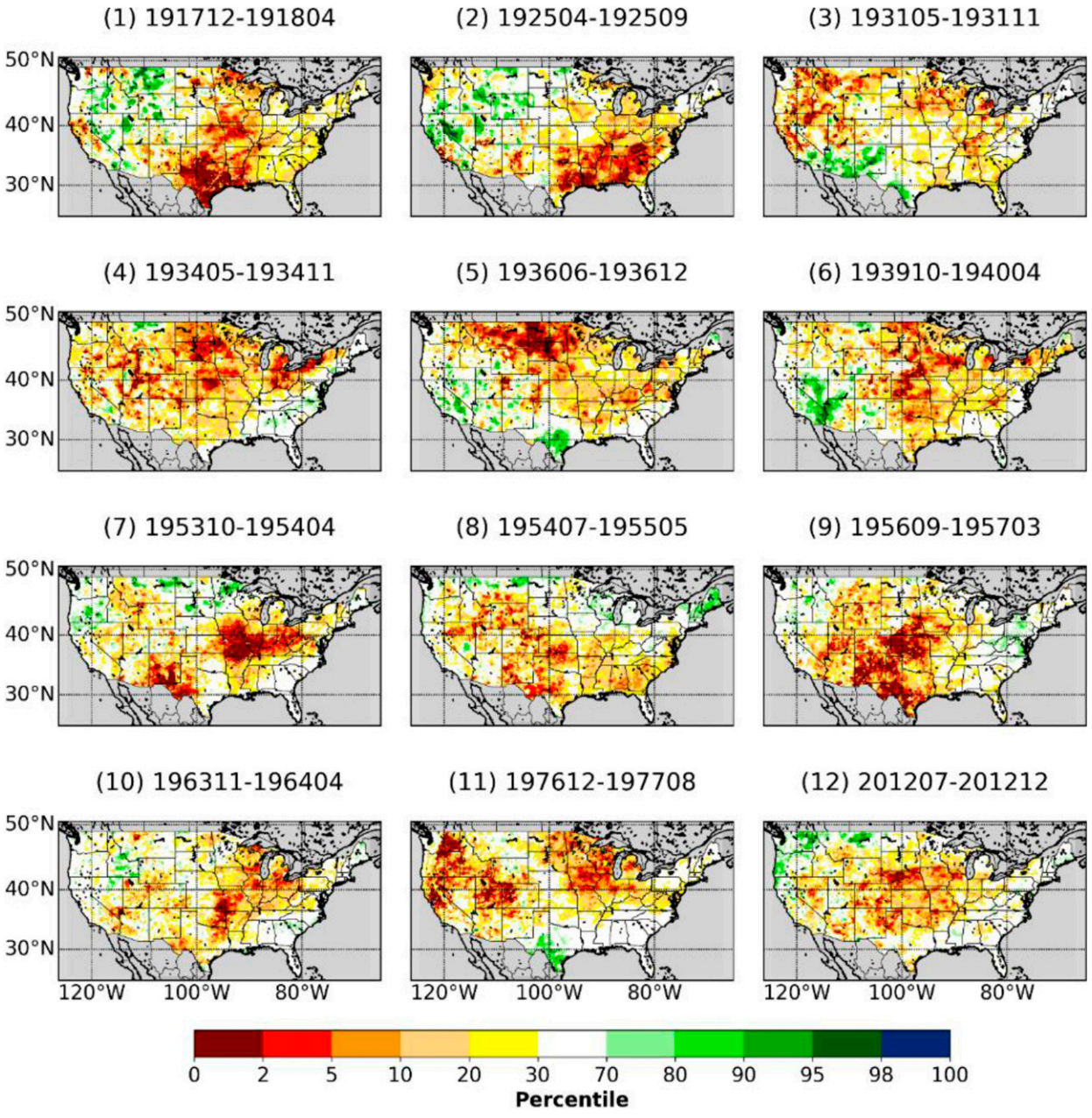

FIG. 2. SM percentiles in BASE averaged over the duration of each event listed in Table 2.

showed that more such events tend to be centered in the central United States than would be expected by chance.

As shown in Table 2, all 12 of the events covered at least 36% of the CONUS (averaged over their durations). The 1934 event was especially widespread; it had a mean spatial extent of about 52% of the CONUS and a peak coverage of 60% in August 1934. Another widespread drought was in 1956 with a mean coverage of 48% and peak coverage of 53%. Even though the 2012 event was the most widespread of the past 40 years, its spatial coverage was somewhat less than most of the other great drought events identified during the longer 1915–2018 period covered here. This underscores the importance of longer term reconstructions to capture more extreme droughts. Among the 12 events whose average severity (spatially averaged monthly SM percentiles over the duration of that event within the maximum spatial extent) ranged from 14.4 to 21.7, the 1934 drought was the most severe. The peak monthly severity ranges around 6th–9th percentiles and the minimum monthly severity ranges around 17th–31st percentiles. As for the drought durations, 11 out of the 12 events lasted for at least 6 months and half of the events lasted for 7 months. The longest of the events (July 1954–May 1955) lasted for 11 months.

When comparing the drought conditions in different runs and outputs (Table S1), we found that the durations of the

great droughts were mostly quite similar. However, three droughts (1931, 1939, and 1956) in GWWA were longer and had earlier onset than in BASE. The difference in 1939 drought onset time is only one month, so here we focus on the 1931 and 1956 droughts for which onset differences were larger. One way in which GWWA results in earlier onset is drought reemergence after (apparent) short-lived drought recovery. In the 1931 event, it had been dry since August 1930 with initial dry area coverage over 42%; however, increased precipitation in October and November 1930 relieved the dry condition (in SM), but left a deficit in groundwater. Before long, the widespread dry condition came back in January 1931. Increased precipitation in March 1931 relieved the dry condition in terms of SM, thus resulting in a break in the drought. Therefore, the 1931 great drought did not occur until May 1931 when only SM is considered in BASE (note that we require great droughts to last for at least five months continuously). However, the increased precipitation in March 1931 did not recharge the GW especially after the earlier dry period in fall 1930; thus, there was no recovery when considering SM and GW, so using GWWA the drought lasted from January 1931 through November 1931. Similarly, increased precipitation in April and July 1956 relieved dry conditions in SM, but failed to recover the GW deficit caused by the earlier drought; thus, the 1956 drought started on April 1956 in GWWA but not until September 1956 in BASE. Furthermore, the GWWA deficit in the 1956 drought was large enough that it deferred the demise by a month in GW relative to BASE.

We found that more than two-thirds of the great droughts tended to have relatively smaller maximum spatial coverage (and average spatial coverage, not shown here) in DYVEG2, GW, and DVGW compared with BASE (Table S1). The coverage fraction differences ranged from 1% to 7%, mostly ≤3%). We found that most of the great droughts tended to have lower severity in GWWA than in BASE, especially in terms of the duration averaged severity $\overline{S}$ (Table S1). DYVEG2 and DVGW also showed somewhat lower severity than BASE generally. Four out of seven great droughts identified in DVGW had smaller average spatial area coverage than DYVEG2 or GW or BASE, which indicates that combined dynamic vegetation phenology and groundwater had synergistic effects in mitigating drought coverage in these four events. DYVEG5 did not show a consistently different patterns compared with BASE, which is most likely because of their similar LAI. BASE assumes fixed vegetation conditions for each year, and leads to higher ET loss estimates in dry years, and hence larger soil moisture deficits, whereas dynamic phenology simulates changes in leaf area according to temperature, soil moisture availability and antecedent LAI, which should more realistically represent drought-induced vegetative stress. Further, BASE assumes free drainage which neglects the effects of groundwater, while under GW configuration, the interaction between soil moisture and shallow groundwater can reflect a more realistic characterization. Therefore, the use of GW and DYVEG configurations arguably should provide a more accurate representation of drought conditions.

We note that the 12 great droughts identified in this study are fewer than in Mo and Lettenmaier (2018) who conducted a somewhat similar analysis and identified 16 events in the period 1916–2013. This is mostly because our threshold (20%) was more stringent than theirs (30%). For the same reason, the spatial coverage and temporal duration of the common events are smaller in our study compared to Mo and Lettenmaier (2018). Most of our great droughts are among those identified in Mo and Lettenmaier (2018) except the 1977 drought, which can be the result of different forcings used in the two studies, as well as the fact that Mo and Lettenmaier (2018) used a different model [Variable Infiltration Capacity (VIC)] whereas we used Noah-MP.

d. *Drought duration analysis*

Apart from great droughts, relatively smaller (compared with the great droughts) but more frequent droughts also can have substantial impacts (note that these are nonetheless longer than what typically are thought of as flash droughts; see, e.g., Pendergrass et al. 2020). Duration is an important factor that determines such impacts but the duration of these smaller (which we term ''major'') droughts over CONUS has not been addressed in previous studies (e.g., Mo and Lettenmaier 2018; Andreadis et al. 2005). Here we evaluate the inferred duration of major droughts, as they are impacted by inclusion of dynamic vegetation and groundwater representations in Noah-MP. Because our interest is in droughts that cover a substantial part of the CONUS domain, we limit our consideration to drought events with minimum areal coverage greater than the 70th percentile of each run's dry area over our study period. Individual short-duration droughts tend to recover more quickly and have less serious impacts; thus, we calculated the 3-month moving average areal coverage for each run. In this way, we screened out short-duration and stand-alone droughts. After that, we identified the months when the dry area coverage was greater than the 70th percentile over the study period. Then we computed the duration of each drought event (separate drought events must have at least a 1-month interval between them). We should note that the criteria here are less stringent than in the great droughts identification where we require the drought area coverage to be higher than the 90th percentile and to last for at least five months. The frequency distribution of major drought durations is shown in Fig. 3. As expected, these shorter droughts have higher frequencies. It should be noted that since we calculated the 3-month moving average of areal coverage, we screened out many (about 50) 1-month ''droughts,'' which is why the 1-month drought frequency is low. In the BASE run, we have 45 major drought events (with a dry area coverage greater than 23.6% of CONUS) with the mean duration of 8.3 months and the longest duration of 58 months. The median drought duration is 4 months, and the 75th and 90th percentiles are 13 and 19 months, respectively. Because the criteria we used are less stringent than in our great drought identification, the mean drought lengths are longer.

The frequency distribution statistics in the GW run are almost the same as in the BASE run (Fig. 3). This is not surprising as the dry areal fraction time series of GW and BASE runs shown in Fig. 1 are very similar. However, this changes when we consider the sum of groundwater and SM as shown in

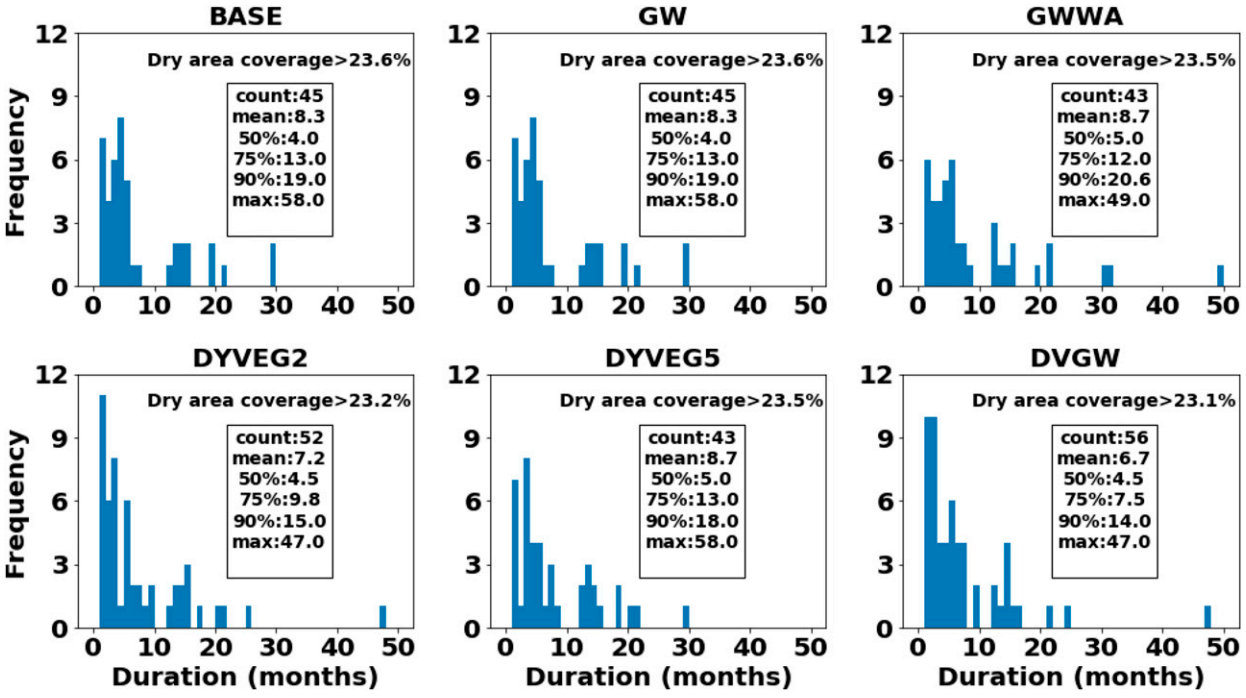

FIG. 3. Frequency distributions of drought duration for BASE, GW (drought calculated based only on SM), GWWA (drought calculated based on SM + GW), DYVEG2, DYVEG5, and DVGW. Only 3-monthly moving average of areal coverage higher than the 70th percentile were retained. The count; mean; 50th, 75th, and 90th percentiles; and the maximum of drought duration (in months) are shown in each subfigure.

Fig. 3c. The areal coverage threshold (23.5%) for drought in GWWA is similar as in BASE (23.6%), but GWWA has a larger mean and 90th percentile durations and shorter 75th percentile and maximum durations than BASE. The contribution of groundwater increases the duration of long-term (90th percentile) droughts by delaying drought recovery and possibly combining shorter droughts into longer ones. The extension of drought recovery is seen in many events. We find that four out of the five longest major droughts end at least one month later in GWWA compared with BASE. This likely occurs because groundwater represents long-term deep water storage, the anomalies in which lag behind precipitation and SM anomalies. Groundwater recovery also tends to be later than SM drought recovery (Bloomfield and Marchant 2013).

In contrast to GWWA, the mean, the maximum, and the 75th and 90th percentiles in DYVEG2 are all smaller than in BASE for major droughts. More than half of the ten longest major droughts have demise time at least a month earlier in DYVEG2 than in BASE. Dynamic vegetation acts as a drought buffer as the dynamic vegetation parameterization tends to "shut down" ET more during dry conditions than does the static (BASE) parameterization, which leads to quicker drought recoveries. It also may be the case that the effect of dynamic vegetation breaks down longer droughts into shorter ones, as evidenced by the higher drought count (52) than in BASE (45). However, the mean, median, 75th and 90th percentiles, and max durations in DYVEG5 are all greater than in DYVAEG2, which likely results from the higher simulation of LAI in DYNAGVEG5 compared with DYNAVEG2 which leads to higher ET loss and more severe apparent droughts. The differences between DYVEG2 and DYVEG5 suggest that the Noah-MP dynamic vegetation options will require careful examination and appropriate application, including parameter specification, before operational use. In DVGW, we see a further decrease in the mean and the 75th and 90th percentiles compared with DYVEG2. Since the drought duration distribution in GW is almost the same as in BASE, this suggests that the effect of groundwater on soil moisture relative to drought duration is enhanced by the inclusion of dynamic vegetation.

e. Subregional drought duration

We further analyzed drought durations in six subregions of CONUS as shown in Fig. 4 (NW = northwest; NC = north central; NE = northeast; SW = southwest; SC = south central; SE = southeast) for major droughts using the same methods as in section 4d. The median drought durations are summarized in Fig. 5. Among all the subregions, SW has the longest drought durations; while SE has the shortest drought durations—not surprisingly following variations in mean precipitation. We also compared the effects of dynamic vegetation and groundwater on drought duration by subregions (Fig. 5). Drought medians are greater in GWWA relative to BASE in SW and SC, mostly due to later drought demise; this is probably because the deep groundwater levels in those regions take longer for drought recovery. Drought durations in NE and NW are shorter in GWWA relative to BASE. In those subregions, it appears that shallow groundwater in the model recharges soil

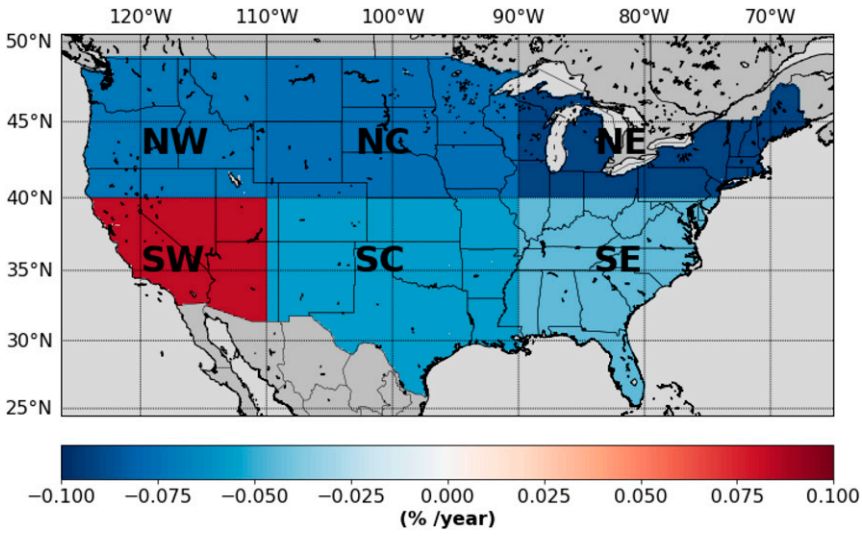

FIG. 4. Six subregions of CONUS: southwest (SW), south central (SC), southeast (SE), northwest (NW), north central (NC), and northeast (NE). The colors denote the trends of dry area coverage for each subregion over our study period in BASE. All the trends are statistically significant (significance level of 0.05).

moisture under dry conditions, therefore mitigating the drought. We found shorter drought duration medians in SW, NC, and NE in both DYVEG2 and DYVEG5. The vegetation types in SW, NC, and NE are mostly shrubs, grassland, and cropland, respectively (see Fig. S9). Under extreme dry conditions, LAI of these vegetation types contract under dynamic vegetation simulations resulting in smaller ET compared with in BASE. This effectively mitigates drought effects, and shortens drought duration compared with in BASE. We also found that the 75th percentiles and maximum values may have different change patterns than the median which indicates a complex influence of groundwater and dynamic vegetation on droughts of different durations and in different regions.

f. Trends in dry area coverage

We examined trends in dry area coverage (based on a grid cell-by-grid cell analysis, i.e., independent of our great and major flood analysis) over the entire CONUS for the past century using the Mann–Kendall statistical test (Mann 1945; Kendall 1975). We found that in all experiments, the CONUS dry area decreased with small Theil–Sen slopes from about -0.04% to $-0.06\%\ \mathrm{yr}^{-1}$ (trends in all experiments are statistically significant at $\alpha = 0.05$). We also examined trends in different subregions (Fig. 4; the time series is shown in Fig. S12), which showed that all subregions except SW had slight decreasing trends (statistically significant for all subregions at $\alpha = 0.05$). The largest (in absolute value) decreasing trend was in NE (from -0.08% to $-0.10\%\ \mathrm{yr}^{-1}$) and the smallest trend was in SE (from -0.04% to $-0.05\%\ \mathrm{yr}^{-1}$). This wetting trend outside of SW is consistent with the general increase in precipitation in the same area for the latter half of the twentieth century (Andreadis and Lettenmaier 2006). In contrast to the other regions, SW showed an increasing trend in dry area coverage (0.06%–0.11%). This drying trend in SW appears to be partly attributable to reduced strength of summer North American monsoon rainfall (Mo and Lettenmaier 2018). It is also partly attributable to the decreased winter precipitation toward the end of our study period. For example, the postmillenium drought in the Colorado River basin was caused primarily by pervasive low-precipitation anomalies across the upper Colorado River basin, and the drought was also exacerbated by negative precipitation anomalies in several of the most productive headwater basins (Xiao et al. 2018). Our findings are consistent with Mo and Lettenmaier (2018). They used an integrated drought index (IDI) and found that the north-central and northeast subregions of CONUS have become wetter while the southwest has become drier. The trends are also supported by Andreadis and Lettenmaier (2006), who studied soil moisture (SM) and runoff (RO) trends in the twentieth century over the CONUS and found that, with the exception of the Southwest and a small portion of the broader western United States, the CONUS has become wetter, with droughts occurring less often and having reduced severity in

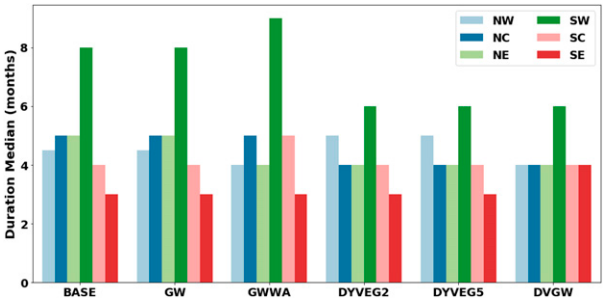

FIG. 5. Median drought durations for different model runs or outputs and subregions.

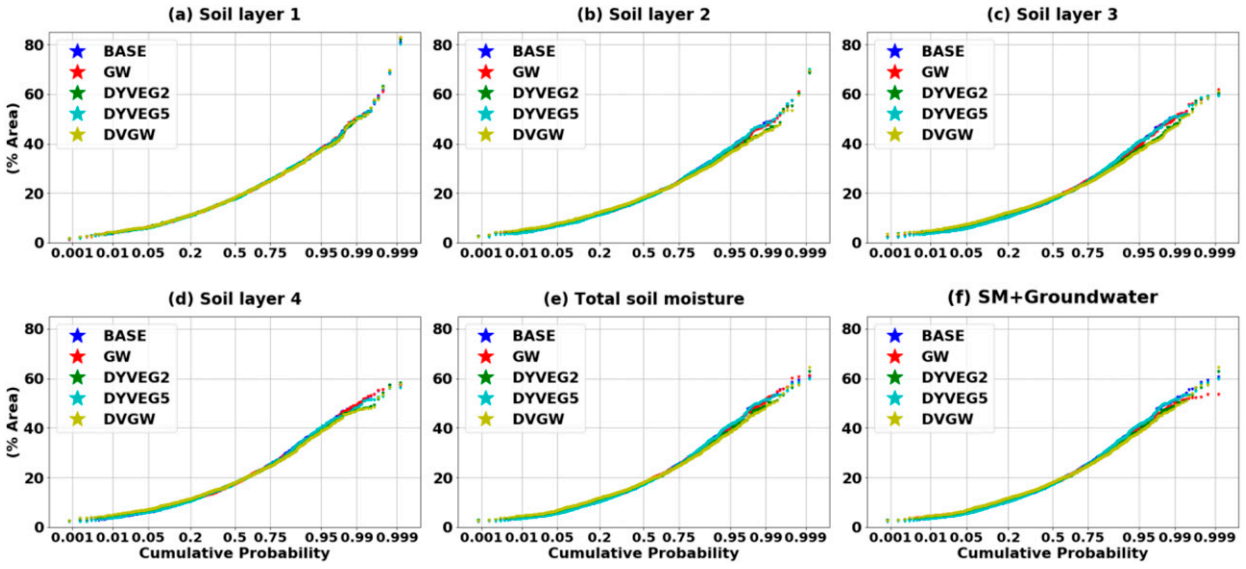

FIG. 6. CDFs of dry area coverage for (a)–(d) soil layers 1–4, (e) CDF of dry area coverage for total soil moisture, and (f) CDF of dry area coverage for total soil moisture + groundwater. Each point corresponds to a monthly averaged dry area coverage in simulations from 1915 to 2018.

recent decades. We also examined the effects of dynamic vegetation phenology and groundwater on the trends. All experiments showed consistent trends in different regions but with varying magnitudes. Over the entire (CONUS) domain, the largest decreasing trend was in BASE, with slightly smaller (in absolute value) trends for both dynamic vegetation phenology and groundwater. Trends for the dynamic vegetation runs were smaller (in absolute value) in all regions except SC. Trends for the groundwater runs were smaller (in absolute value) in NC, SC, SE, and CONUS as a whole, but were larger (in absolute value) in SW, NE, and NW.

g. Variations by soil layers

In Noah-MP, the soil column is divided into four layers with thicknesses of 0.1, 0.3, 0.6, and 1.0 m from the surface to the bottom (total depth is fixed at 2 m throughout the domain). Since dynamic vegetation and groundwater should affect soil moisture differently depending on the soil depth, we examined the cumulative distribution function (CDF) of dry area coverage for different soil layers and for different experiments (Fig. 6). Noah-MP assumes static uniformly distributed roots vertically and varying rooting depths depending on vegetation type. For example, the roots for cropland, grassland, and shrubland are assumed to be present in the upper three soil layers (top 1 m), whereas in forests they are present in four layers (2 m). Generally, the dry area coverage for extreme droughts (CDF $>$ 0.99) decreases as the soil depth increases, ranging from ~50%–80% for soil layer 1 to ~50%–60% for soil layer 4 (Figs. 6a–d). This is because soil moisture in lower layers is more weakly linked with the surface than in the upper layers, which results in smaller dry area coverage as depth increases. This is more significant for short vegetation (shrubs, crop, grass, etc.) (Fig. S13) than forests (Fig. S14).

In soil layer 1 (Fig. 6a), the CDFs for different experiments are quite similar. The differences are more apparent in layers 2, 3, and 4, and are most significant in layer 3 (Figs. 6c–e). Generally, the baseline is more similar to GW and DYVEG5, while DYVEG2 is similar to DVGW, which suggests that dynamic vegetation has a greater influence on SM than does GW. For higher CDFs, BASE, GW, and DYVEG5 generally have larger dry area coverage than DYVEG2 and DVGW. In layer 2, the CDFs begin to diverge for large values ($>$~0.96) but converge for very high CDFs. In layer 3, the CDFs begin to diverge for values $>$ ~0.82 but also converge for very large CDFs. In layer 4, the CDFs diverge only for CDF greater than about 0.97, and as for the other layers, converge for very large CDF.

An explanation for this behavior is that greater differences occur in the middle (layers 2 and 3) than in the surface or bottom layers, because soil layer 1 is shallow and tends to become saturated or dried out easily (i.e., is in close communication with the atmospheric forcings) and thus is less sensitive to variations in groundwater or vegetation. For most vegetation types, most of the roots are present in soil layers 2 and 3 (0.1–1.0 m) and moisture in this depth range is therefore more sensitive to dynamic vegetation changes than near the surface. This is especially true for short vegetation whose roots are in the upper three layers and contract in extreme droughts under the dynamic vegetation phenology configuration. Contracted vegetation decreases ET and thus mitigates extreme droughts in areas with shorter vegetation roots, as is apparent in Fig. S13. However, forests generally do not contract under droughts and thus are less sensitive to dynamic phenology (Fig. S14). However, soil layer 4 is too deep (1.0–2.0 m) for roots to extract moisture for crops, grass, and shrubs and thus it has smaller responses to dynamic vegetation phenology (only forests' roots reach down into layer 4).

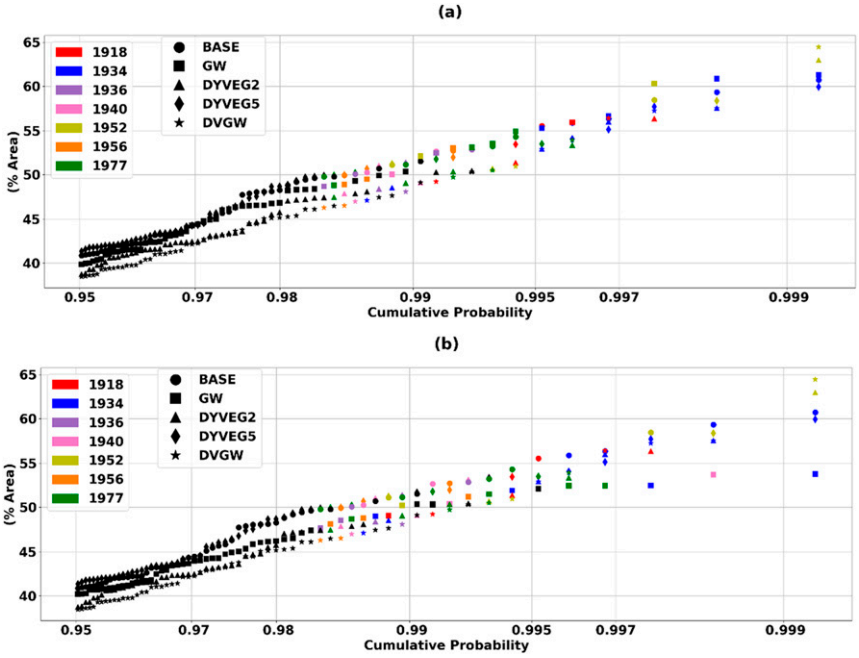

FIG. 7. CDFs of dry area coverage (for CDF > 0.95) based on (a) total soil moisture and (b) total soil moisture + groundwater for the GW run. For both plots, each point denotes a value for the monthly averaged dry area coverage over the period 1915–2018.

Total SM (Fig. 6e) shows similar patterns as for the lower layers (Figs. 6b–d) and the CDF for GW does not separate from the BASE CDF. The CDF for total SM + GW (Fig. 6f), for the GW run separates from the other CDFs with dry area coverage becoming nearly constant at 52% for large CDF. This is shown more clearly in Fig. 7 which expands the results for CDF greater than 0.95. The smaller dry area spatial coverage in GW shown in Figs. 7a and 7b makes clear that GW mitigates extreme droughts. Examination of the results show that the largest dry area coverages (which are most affected by GW) are in the 1930s, 1950s, and 1977.

h. Effects of dynamic vegetation phenology and groundwater for specific droughts

To understand the effects of dynamic vegetation phenology on droughts, we examined some specific cases. Figure 8 shows the SM percentiles on 1 August 1934, while Fig. 9 shows corresponding LAI values. We also show the vegetation volume (defined as FVEG × LAI) for different runs in Fig. S15; they show similar patterns to LAI. As noted above, the dry area coverage for the 1934 drought is high, about 60.7% in BASE, 57.5% in DYVEG2, and 60.0% in DYVEG5. The largest difference between BASE (Fig. 8a) and DYVEG2 (Fig. 8b) is in the north central part of the domain. We found that the LAI in DYVEG2 (Fig. 9b) is much lower than in BASE (Fig. 9a, which uses a monthly climatology LAI table by vegetation type). The apparent explanation is that for this extreme dry and hot situation, the dynamic vegetation phenology in DYVEG2 kills vegetation, which lowers the ET, and allows soil moisture to recover. In contrast, in DYVEG5, the LAI (Fig. 9c) is similar to BASE, and the drought condition is almost the same (Figs. 8a,c). Similar patterns are shown in the vegetation volume (Fig. S15). As discussed above, the LAI simulation in the two dynamic vegetation phenology configurations is most different in cropland where LAI is very low in DYVEG2 and much higher in DYVEG5 (Fig. S8). The difference is especially

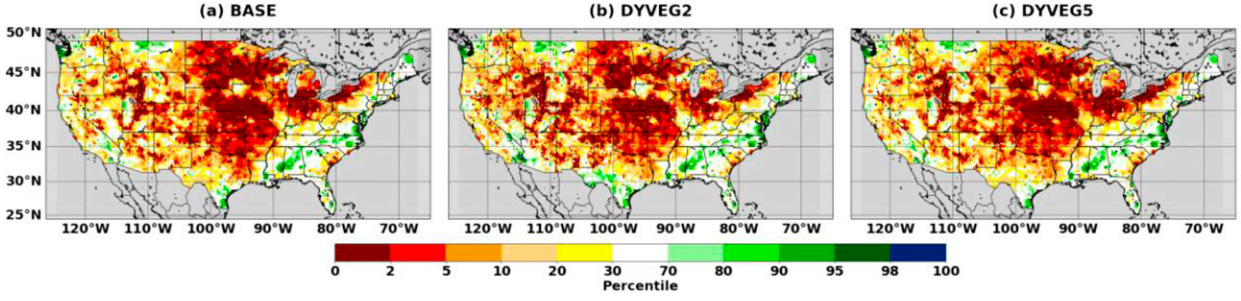

FIG. 8. Total soil moisture percentiles on 1 Aug 1934 for (a) BASE, (b) DYVEG2, and (c) DYVEG5.

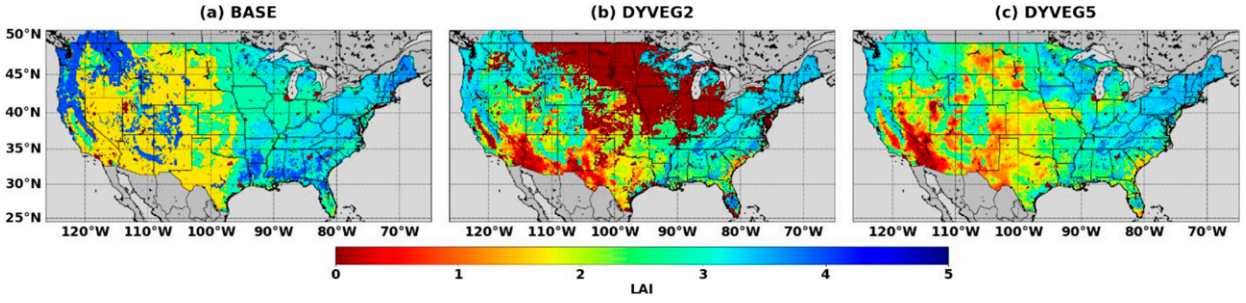

FIG. 9. Leaf area index on 1 Aug 1934 for (a) BASE, (b) DYVEG2, and (c) DYVEG5.

apparent in the north central CONUS which is dominated by croplands (Figs. 9b,c) and thus results in the difference in central north between DYVEG2 and DYVEG5.

Similar behavior occurs on 1 October 2015 (Figs. 10, 11 and Fig. S16), which was near the end of an epic drought in California, which had spread to much of the West. The dry area coverage is about 16.1% in BASE, 27.2% in DYVEG2, and 15.6% in DYVEG5. Again, the dry conditions in BASE (Fig. 10a) are similar to DYVEG5 (Fig. 10c); however, for this case DYVEG2 (Fig. 10b) is drier than BASE. The main differences in this case are in the West, where LAI in DYVEG2 (Fig. 11b) is higher than in BASE (Fig. 11a). In DYVEG2, the drought does not reduce LAI in the West, and higher vegetation yields more ET which exacerbates the western U.S. drought (which was then in its final stage). The LAI in north central CONUS in October 2015 was quite similar to that in August 1934 in DYVEG2 since the LAI simulation in cropland remained low during the study period in DYVEG2 (Fig. S8).

We also examined the effects of groundwater on drought classification. A good example is the recovery at the end of the prolonged 2012–16 California drought (Fig. 12). The top 1-m SM (Figs. 12a,b) in BASE indicates that the drought in California was fully recovered on 3 January 2017. But GW (Figs. 12c,d) shows that, when GWWA is used as a drought indicator, the drought had not yet completely ended, especially in southern California. This in fact matches well with USDM, which indicated that the drought was not completely gone until 7 February 2017. This example suggests that groundwater storage was reduced in this extreme drought event, and the groundwater reduction exacerbated the effects of the drought by prolonging the drought recovering process, despite several major storm events which saturated the upper 1 m or so of the soil column. The groundwater physics in Noah-MP represents these processes. Despite recoveries across much of the state, the longer-term impacts of the drought were still being observed relative to groundwater supplies in various California locations in winter 2017 (USDM 2017).

We should note that model uncertainties in representing groundwater-soil water exchange and vegetation dynamics undoubtedly affect our results. Especially notable are the effects of Noah-MP's relatively simple representation of ecosystem effects on the processes and variables we use for drought characterization. For instance, plants are able to adjust water use efficiency (WUE) according to water availability. Higher WUE is likely in drier years and is likely to increase as droughts evolve, thus enhancing ecosystem resilience to droughts (Ponce-Campos et al. 2013; Huxman et al. 2004). Furthermore, in semiarid areas where droughts are common, there has been an increase in greenness in recent decades (Ahlstrom et al. 2015). Thus, the ability of Noah-MP's dynamic vegetation parameterization to reproduce ecosystem effects can have a major influence on its ability to replicate drought behavior. In this respect, the (current) version of Noah-MP used in this study does not necessarily well represent plant hydraulics and ecosystem resilience. Furthermore, groundwater capillary rise as represented in the current version of Noah-MP may be too weak due to the low content of soil micropore volume (micropore content is fixed at 0.2). Since the state and variability of soil moisture are sensitive to the magnitude of soil micropore volume and generally, a larger micropore volume produces a wetter soil with a smaller soil moisture variability

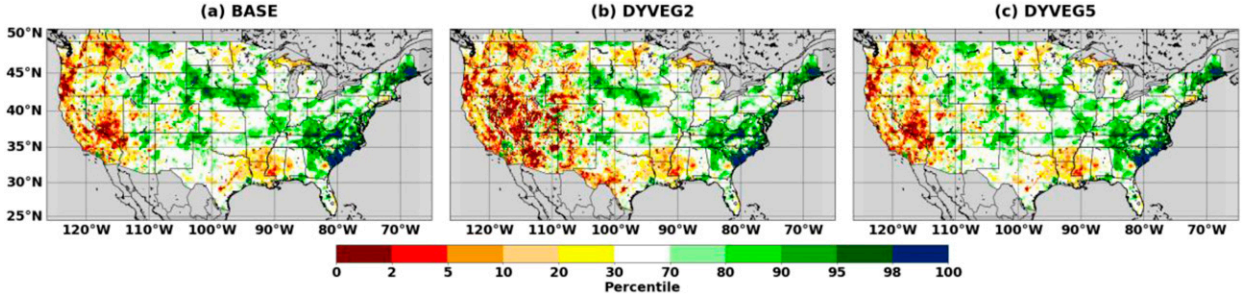

FIG. 10. Total soil moisture percentiles (%) on 1 Oct 2015 for (a) BASE, (b) DYVEG2, and (c) DYVEG5.

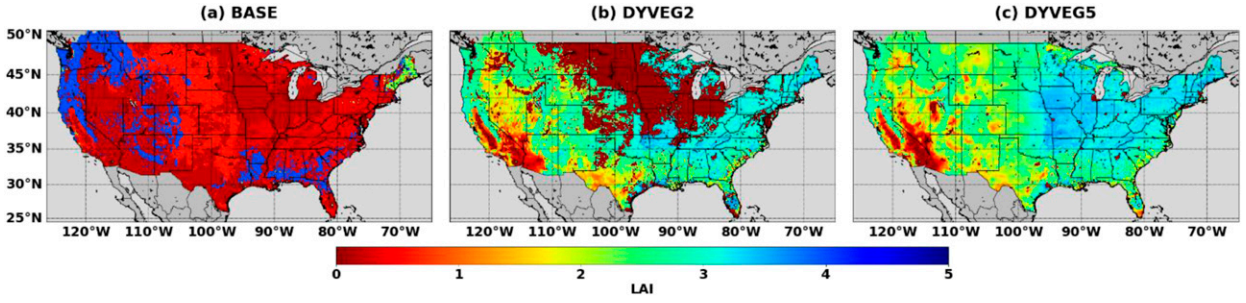

FIG. 11. Leaf area index on 1 Oct 2015 for (a) BASE, (b) DYVEG2, and (c) DYVEG5.

(Niu et al. 2011), the low micropore can generate drier conditions.

5. Conclusions

We examined drought variability over CONUS for the century-long period 1915–2018 using the Noah-MP LSM and evaluated the effects of dynamic vegetation phenology and groundwater. Our key findings are as follows:

1) Twelve great droughts occurred over the 104-yr reconstruction period that covered at least 36% of CONUS and lasted for at least 5 months.
2) Forty-five major drought events occurred in the BASE (with a dry area coverage greater than 23.6% of CONUS) with mean duration 8.3 months and longest duration 58 months. The Southwest (Southeast) has the longest (shortest) major drought durations.
3) Representation of groundwater effects tends to increase drought duration (for some, but not all, of both great droughts and major droughts), primarily by leading to earlier drought onset (associated with short-lived recovery from a previous drought) or later demise (groundwater anomalies lag precipitation anomalies). In contrast, representation of dynamic vegetation phenology tends to shorten major drought durations, primarily by earlier demise. Compared with the fixed vegetation indices used in most previous studies, dynamic vegetation phenology acts as a buffer to drought as it reflects the fact that water loss from ET reduces in drought due to closed stoma or dead vegetation. Groundwater and dynamic vegetation phenology also tend to contribute to lower drought severity and smaller spatial coverage for great droughts.
4) Statistically significant decreasing trends in dry area coverage occurred over most of CONUS over the past century,

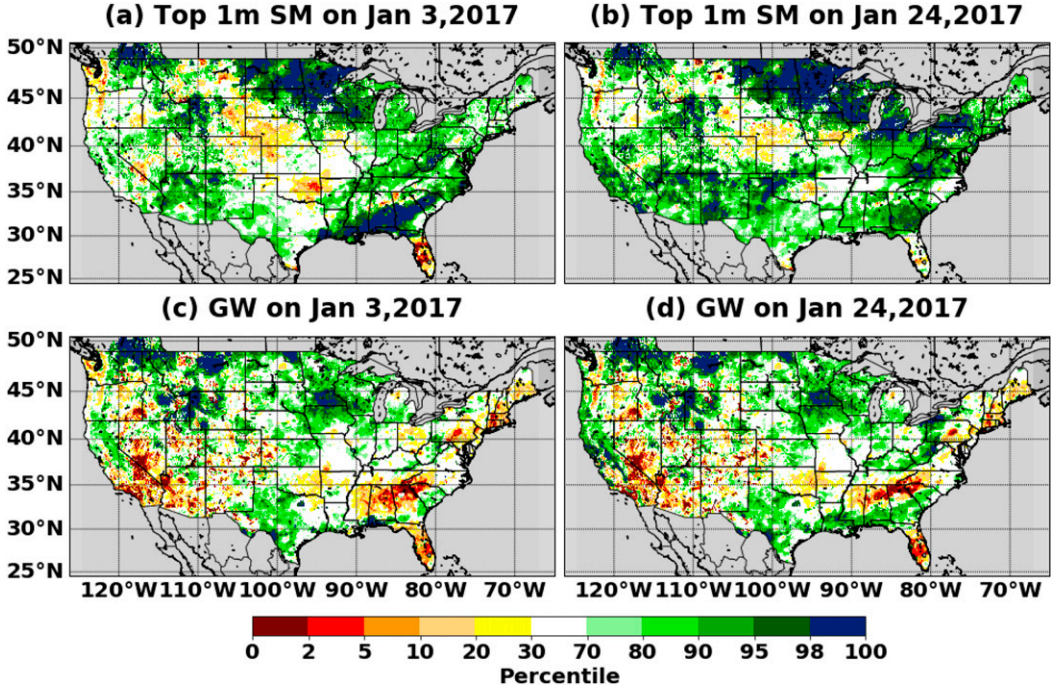

FIG. 12. (a) Top 1-m soil moisture percentiles on 3 Jan 2017 in BASE. (b) As in (a), but for 24 Jan 2017. (c) Groundwater percentiles on 3 Jan 2017 and (d) groundwater percentiles on 24 Jan 2017.

and are evident in all the model configurations. The exception is SW, where (statistically significant) increasing trend in dry area coverage occurred over our study period.

5) Dynamic vegetation phenology has a greater influence on soil moisture in the two middle model layers than on either top or bottom layers. This is especially true for short vegetation whose roots occupy the upper soil layers and contract in great droughts thus serving as a negative feedback which mitigates drought severity.

Acknowledgments. This work was supported by the NOAA/MAPP Grant NA17OAR4310146 to the University of California, Los Angeles. All authors were supported by separate grants from NOAA's Modeling and Predictions Program and are members of the NOAA MAPP Drought Task Force. C.D.P-L. and D.M.M. were partially supported by NASA's Terrestrial Hydrology Program.

Data availability statement. The extended forcings used in this study are openly available at ftp://livnehpublicstorage.colorado.edu/public/sulu/extended_PrecTminTmaxWind_2012_2018/.The outputs that support the findings of this study are openly available at https://figshare.com/articles/Drought_variability_over_CONUS_for_the_past_century/12560216.

REFERENCES

Ahlstrom, A., and Coauthors, 2015: The dominant role of semiarid ecosystems in the trend and variability of the land CO_2 sink. *Science*, **348**, 895–899, https://doi.org/10.1126/science.aaa1668.

Ahmadalipour, A., H. Moradkhani, and M. Svoboda, 2017: Centennial drought outlook over the CONUS using NASA-NEX downscaled climate ensemble. *Int. J. Climatol.*, **37**, 2477–2491, https://doi.org/10.1002/joc.4859.

Andreadis, K. M., and D. P. Lettenmaier, 2006: Trends in 20th century drought over the continental United States. *Geophys. Res. Lett.*, **33**, L10403, https://doi.org/10.1029/2006GL025711.

——, E. A. Clark, A. W. Wood, A. F. Hamlet, and D. P. Lettenmaier, 2005: Twentieth-century drought in the conterminous United States. *J. Hydrometeor.*, **6**, 985–1001, https://doi.org/10.1175/JHM450.1.

Ball, J. T., I. E. Woodrow, and J. A. Berry, 1987: A model predicting stomatal conductance and its contribution to the control of photosynthesis under different environmental conditions. *Progress in Photosynthesis Research*, Vol. 4, J. Biggins, Ed., Martinus Nijhoff, 221–224.

Barlage, M., M. Tewari, F. Chen, G. Miguez-Macho, Z. Yang, and G. Niu, 2015: The effect of groundwater interaction in North American regional climate simulations with WRF/Noah-MP. *Climatic Change*, **129**, 485–498, https://doi.org/10.1007/s10584-014-1308-8.

Bloomfield, J. P., and B. P. Marchant, 2013: Analysis of groundwater drought building on the standardised precipitation index approach. *Hydrol. Earth Syst. Sci.*, **17**, 4769–4787, https://doi.org/10.5194/hess-17-4769-2013.

Bohn, T. J., B. Livneh, J. W. Oyler, S. W. Running, B. Nijssen, and D. P. Lettenmaier, 2013: Global evaluation of MTCLIM and related algorithms for forcing of ecological and hydrological models. *Agric. For. Meteor.*, **176**, 38–49, https://doi.org/10.1016/j.agrformet.2013.03.003.

Bras, R. L., 1990: *Hydrology: An Introduction to Hydrologic Science*. Addison-Wesley, 643 pp.

Cai, X., Z. L. Yang, C. H. David, G. Y. Niu, and M. Rodell, 2014: Hydrological evaluation of the Noah-MP land surface model for the Mississippi River Basin. *J. Geophys. Res. Atmos.*, **119**, 23–38, https://doi.org/10.1002/2013JD020792.

Chen, F., and Coauthors, 1996: Modeling of land-surface evaporation by four schemes and comparison with FIFE observations. *J. Geophys. Res.*, **101**, 7251–7268, https://doi.org/10.1029/95JD02165.

——, and J. Dudhia, 2001: Coupling an advanced land surface-hydrology model with the Penn State–NCAR MM5 modeling system. Part I: Model implementation and sensitivity. *Mon. Wea. Rev.*, **129**, 569–585, https://doi.org/10.1175/1520-0493(2001)129<0569:CAALSH>2.0.CO;2.

Cosgrove, B., and D. Gochis, 2018: The National Water Model: Overview and Future Development. *USGS National Hydrography Dataset Newsletter*, Vol. 17, No. 6, USGS, Reston, VA, 4–7, https://www.usgs.gov/media/files/nhd-newsletter-201806-june-2018.

Dai, A., K. E. Trenberth, and T. Qian, 2004: A global data set of Palmer drought severity index for 1870–2002: Relationship with soil moisture and effects of surface warming. *J. Hydrometeor.*, **5**, 1117–1130, https://doi.org/10.1175/JHM-386.1.

Daly, C., R. P. Neilson, and D. L. Phillips, 1994: A statistical topographic model for mapping climatological precipitation over mountainous terrain. *J. Appl. Meteor.*, **33**, 140–158, https://doi.org/10.1175/1520-0450(1994)033<0140:ASTMFM>2.0.CO;2.

Dickinson, R. E., M. Shaikh, R. Bryant, and L. Graumlich, 1998: Interactive canopies for a climate model. *J. Climate*, **11**, 2823–2836, https://doi.org/10.1175/1520-0442(1998)011<2823:ICFACM>2.0.CO;2.

Ek, M., and Coauthors, 2011: North American Land Data Assimilation System Phase 2 (NLDAS-2): Development and applications, *GEWEX News*, Vol. 21, No. 2, International GEWEX Project Office, Silver Spring, MD, 6–7, https://www.gewex.org/gewex-content/files_mf/1432209506May2011.pdf.

Fan, Y., 2015: Groundwater in the Earth's critical zone: Relevance to large-scale patterns and processes. *Water Resour. Res.*, **51**, 3052–3069, https://doi.org/10.1002/2015WR017037.

——, H. Li, and G. Miguez-Macho, 2013: Global patterns of groundwater table depth. *Science*, **339**, 940–943, https://doi.org/10.1126/science.1229881.

Ge, Y., T. Apurv, and X. Cai, 2016: Spatial and temporal patterns of drought in the continental US during the past century. *Geophys. Res. Lett.*, **43**, 6294–6303, https://doi.org/10.1002/2016GL069660.

Hughes, J. D., K. C. Petrne, and R. P. Silberstein, 2012: Drought, groundwater storage and stream flow decline in southwestern Australia. *Geophys. Res. Lett.*, **39**, L03408, https://doi.org/10.1029/2011GL050797.

Huxman, T. E., and Coauthors, 2004: Convergence across biomes to a common rain-use efficiency. *Nature*, **429**, 651–654, https://doi.org/10.1038/nature02561.

Kalnay, E., and Coauthors, 1996: The NCEP/NCAR 40-Year Reanalysis Project. *Bull. Amer. Meteor. Soc.*, **77**, 437–472, https://doi.org/10.1175/1520-0477(1996)077<0437:TNYRP>2.0.CO;2.

Kendall, M. G., 1975: *Rank Correlation Methods*. 4th ed. Charles Griffin, 202 pp.

Kimball, J. S., S. W. Running, and R. R. Nemani, 1997: An improved method for estimating surface humidity from daily minimum temperature. *Agric. For. Meteor.*, **85**, 87–98, https://doi.org/10.1016/S0168-1923(96)02366-0.

Livneh, B., E. A. Rosenberg, C. Lin, B. Nijssen, V. Mishra, K. M. Andreadis, E. P. Maurer, and D. P. Lettenmaier, 2013: A long-term hydrologically based dataset of land surface fluxes and states for the conterminous United States: Update and extensions. *J. Climate*, **26**, 9384–9392, https://doi.org/10.1175/JCLI-D-12-00508.1.

Mann, H. B., 1945: Non-parametric tests against trend. *Econometrica*, **13**, 245–259, https://doi.org/10.2307/1907187.

Martinez, J. A., F. Dominguez, and G. Miguez-Macho, 2016: Effects of a groundwater scheme on the simulation of soil moisture and evapotranspiration over southern South America. *J. Hydrometeor.*, **17**, 2941–2957, https://doi.org/10.1175/JHM-D-16-0051.1.

Mitchell, K. E., and Coauthors, 2004: The multi-institution North American Land Data Assimilation System (NLDAS): Utilizing multiple GCIP products and partners in a continental distributed hydrological modeling system. *J. Geophys. Res.*, **109**, D07S90, https://doi.org/10.1029/2003JD003823.

Mo, K. C., 2008: Model-based drought indices over the United States. *J. Hydrometeor.*, **9**, 1212–1230, https://doi.org/10.1175/2008JHM1002.1.

——, and D. P. Lettenmaier, 2018: Drought variability and trends over the central United States in the instrumental record. *J. Hydrometeor.*, **19**, 1149–1166, https://doi.org/10.1175/JHM-D-17-0225.1.

——, L. N. Long, Y. Xia, S. K. Yang, J. E. Schemm, and M. Ek, 2011: Drought indices based on the climate forecast system reanalysis and ensemble NLDAS. *J. Hydrometeor.*, **12**, 181–205, https://doi.org/10.1175/2010JHM1310.1.

Narasimhan, B., and R. Srinivasan, 2005: Development and evaluation of soil moisture deficit index (SMDI) and evapotranspiration deficit index (ETDI) for agricultural drought monitoring. *Agric. For. Meteor.*, **133**, 69–88, https://doi.org/10.1016/j.agrformet.2005.07.012.

Niu, G.-Y., Z. L. Yang, R. E. Dickinson, L. E. Gulden, and H. Su, 2007: Development of a simple groundwater model for use in climate models and evaluation with Gravity Recovery and Climate Experiment data. *J. Geophys. Res.*, **112**, D07103, https://doi.org/10.1029/2006JD007522.

——, and Coauthors, 2011: The community Noah land surface model with multiparameterization options (Noah-MP): 1. Model description and evaluation with local-scale measurements. *J. Geophys. Res.*, **116**, D12109, https://doi.org/10.1029/2010JD015139.

NOAA, 2020: U.S. Billion-Dollar Weather and Climate Disasters. NOAA/NCEI, https://www.ncdc.noaa.gov/billions/.

Pendergrass, A. G., and Coauthors, 2020: Flash droughts present a new challenge for subseasonal-to-seasonal prediction. *Nat. Climate Change*, **10**, 191–199, https://doi.org/10.1038/s41558-020-0709-0.

Peters, E., P. J. J. F. Torfs, H. A. J. Van Lanen, and G. Bier, 2003: Propagation of drought through groundwater—A new approach using linear reservoir theory. *Hydrol. Processes*, **17**, 3023–3040, https://doi.org/10.1002/hyp.1274.

——, H. A. J. Van Lanen, P. J. J. F. Torfs, and G. Bier, 2005: Drought in groundwater—Drought distribution and performance indicators. *J. Hydrol.*, **306**, 302–317, https://doi.org/10.1016/j.jhydrol.2004.09.014.

Ponce-Campos, and Coauthors, 2013: Ecosystem resilience despite large-scale altered hydroclimatic conditions. *Nature*, **494**, 349–352, https://doi.org/10.1038/nature11836.

Schaake, J., S. Cong, and Q. Duan, 2006: The US Mopex data set. *IAHS Publ.*, **307**, 9–28, https://iahs.info/uploads/dms/13600.04-9-28-SCHAAKE.pdf.

Svoboda, M., and Coauthors, 2002: The Drought Monitor. *Bull. Amer. Meteor. Soc.*, **83**, 1181–1190, https://doi.org/10.1175/1520-0477-83.8.1181.

Tang, Q., E. R. Vivoni, F. Muñoz-Arriola, and D. P. Lettenmaier, 2012: Predictability of evapotranspiration patterns using remotely sensed vegetation dynamics during the North American monsoon. *J. Hydrometeor.*, **13**, 103–121, https://doi.org/10.1175/JHM-D-11-032.1.

Thornton, P. E., and S. W. Running, 1999: An improved algorithm for estimating incident daily solar radiation from measurements of temperature, humidity, and precipitation. *Agric. For. Meteor.*, **93**, 211–228, https://doi.org/10.1016/S0168-1923(98)00126-9.

USDM, 2017: Summary for 31 January 2017. U.S. Drought Monitor, https://droughtmonitor.unl.edu/Summary.aspx.

Verstraeten, W. W., F. Veroustraete, and J. Feyen, 2008: Assessment of evapotranspiration and soil moisture content across different scales of observation. *Sensors*, **8**, 70–117, https://doi.org/10.3390/s8010070.

Wang, A., T. J. Bohn, S. P. Mahanama, R. D. Koster, and D. P. Lettenmaier, 2009: Multimodel ensemble reconstruction of drought over the continental United States. *J. Climate*, **22**, 2694–2712, https://doi.org/10.1175/2008JCLI2586.1.

Wilhite, D. A., 2006: Drought monitoring, mitigation and preparedness in United States: An end to end approach. *WMO Task Force on Social-Economic Application of Public Weather Services*, Geneva, Switzerland, WMO, 32 pp., https://www.wmo.int/pages/prog/amp/pwsp/documents/Wilhite_WMO_Drought_PWS.pdf.

Wu, J., C. Miao, H. Zheng, Q. Duan, X. Lei, and H. Li, 2018: Meteorological and hydrological drought on the Loess Plateau, China: Evolutionary characteristics, impact, and propagation. *J. Geophys. Res. Atmos.*, **123**, 11 569–11 584, https://doi.org/10.1029/2018JD029145.

Xia, Y. L., and Coauthors, 2012a: Continental-scale water and energy flux analysis and validation for the North American Land Data Assimilation System project phase 2 (NLDAS-2): 1. Intercomparison and application of model products. *J. Geophys. Res.*, **117**, D03109, https://doi.org/10.1029/2011JD016048.

——, and Coauthors, 2012b: Continental-scale water and energy flux analysis and validation for the North American Land Data Assimilation System project phase 2 (NLDAS-2): 2. Validation of model-simulated streamflow. *J. Geophys. Res.*, **117**, D03110, https://doi.org/10.1029/2011JD016051.

Xiao, M., B. Nijssen, and D. P. Lettenmaier, 2016: Drought in the Pacific Northwest, 1920–2013. *J. Hydrometeor.*, **17**, 2391–2404, https://doi.org/10.1175/JHM-D-15-0142.1.

——, B. Udall, and D. P. Lettenmaier, 2018: On the causes of declining Colorado River streamflows. *Water Resour. Res.*, **54**, 6739–6756, https://doi.org/10.1029/2018WR023153.